Numerical simulation of viscoelastic fluid flows with free surfaces

Hugo L. França[1], Cassio M. Oishi[2], José A. Cuminato[1]

[1]*Instituto de Ciências Matemáticas e Computação, Universidade de São Paulo*
Avenida Trabalhador São-carlense, 400, 13566-590, São Carlos, Brazil
franca.hugo1@gmail.com, jacumina@icmc.usp.br
[2]*Departamento de Matemática e Computação, Faculdade de Ciências e Tecnologia, Universidade Estadual Paulista "Júlio de Mesquita Filho"*
Rua Roberto Simonsen, 305, 19060-900, Presidente Prudente, Brazil
cassio.oishi@unesp.br

Abstract. In this work we will present a numerical study of viscoelastic fluid flows under surface tension effects. The mathematical model adopted involves the governing equations for incompressible fluids with free surface, along with the constitutive equations that describe a viscoelastic material. From a computational point of view, the free surface dynamics will be handled using the Front-Tracking representation with marker particles, combined with the Marker-And-Cell (MAC) method to discretize the equations using a finite differences scheme. Our current interest is the study of small-scale flows with droplet impact, such as the collision between two droplets. Viscoelastic models will be adopted in order to represent the non-Newtonian contributions on different post-impact outcomes, e.g., coalescence, separation and bouncing between droplets. Considering the classical dimensionless numbers on viscoelastic free surface flows (Reynolds, Weber and Weissenberg), we will present parametric studies on the simulation of droplet collisions to investigate how these parameters affect the final outcome.

Keywords: Viscoelastic fluids, Free surface flows, Numerical simulation

1 Introduction

Non-Newtonian materials are found in many different industrial applications, such as in oil industry problems, cosmetics, food products, or in biological fluid problems such as hemodynamics. In particular, the modelling of viscoelastic materials have been the subject of many studies due to their complexity and the difficulty in finding appropriate mathematical models.

In the context of computational simulations, an additional challenge is the presence of moving interfaces, such as in free surface or multiphase flows. For free surface flows, it is worth mentioning the recent works of Oishi [1, 2], while for multiphase flows, the work of Izbassarov [3]. In this work we implement and analyse new computational tools in order to also incorporate the effects of surface tension to the viscoelastic models. We also present numerical ideas to handle topological changes that may arise from these complex fluid flows.

In our study, we give special attention to studying problems in which the surface tension has an important role, such as flows involving the impact of very small droplets. We are also particularly interested in simulations that present moving surfaces with topological changes. These changes can be generally classified in two types: fluid breakup or fluid coalescence.

The test problem chosen to illustrate this study was the binary droplet collision, in which two small droplets collide against each other. We chose this particularly problem due to it being heavily influenced by surface tension, presenting very interesting topological changes and because the literature for non-Newtonian fluids is still scarce (especially for viscoelastic fluids).

2 Governing equations

The governing equations for isothermal incompressible flow, are the continuity and momentum equations

$$\rho\left(\frac{\partial \mathbf{u}}{\partial t} + \nabla\cdot(\mathbf{uu})\right) = -\nabla p + \nabla\cdot\boldsymbol{\tau} + \rho\mathbf{g}, \tag{1}$$

$$\nabla\cdot\mathbf{u} = 0, \tag{2}$$

where $\mathbf{u}$ and p are the velocity and pressure fields, respectively, ρ is the fluid density and $\mathbf{g}$ is a source term (usually gravity). The extra-stress tensor $\boldsymbol{\tau}$ is composed of solvent $\boldsymbol{\tau}^s$ and polymer $\boldsymbol{\tau}^p$ contributions, being written as

$$\boldsymbol{\tau} = \boldsymbol{\tau}^s + \boldsymbol{\tau}^p. \tag{3}$$

The solvent contribution represents the Newtonian behaviour of the fluid and is given by

$$\boldsymbol{\tau}^s = 2\eta_s\mathbf{D}, \tag{4}$$

where η_s is the solvent viscosity and $\mathbf{D} = \frac{1}{2}\left(\nabla\mathbf{u} + (\nabla\mathbf{u})^T\right)$ is the rate-of-strain tensor. For viscoelastic fluids, the term $\boldsymbol{\tau}^p$ represents the polymeric contribution in the flow which is generally modelled by a hyperbolic constitutive equation. In particular, if the Oldroyd-B model is adopted, the constitutive equation is

$$\boldsymbol{\tau}^p + \lambda_p \overset{\triangledown}{\boldsymbol{\tau}}^p = 2\eta_p\mathbf{D}, \tag{5}$$

where λ_p is the relaxation time and η_p is the polymer viscosity. The upper-convected derivative $\overset{\triangledown}{\boldsymbol{\tau}}^p$ is defined as

$$\overset{\triangledown}{\boldsymbol{\tau}}^p = \frac{\partial\boldsymbol{\tau}^p}{\partial t} + (\mathbf{u}\cdot\nabla)\,\boldsymbol{\tau}^p - (\nabla\mathbf{u})\boldsymbol{\tau}^p - \boldsymbol{\tau}^p(\nabla\mathbf{u})^T. \tag{6}$$

A non-dimensionalization can be performed by scaling the variables as follows

$$\mathbf{x} = L\bar{\mathbf{x}}, \quad t = \frac{L}{U}\bar{t}, \quad \mathbf{u} = U\bar{\mathbf{u}}, \quad p = \rho U^2\bar{p}, \quad \boldsymbol{\tau}^p = \frac{\eta_0 U}{L}\bar{\mathbf{T}}, \quad \mathbf{g} = g_0\bar{\mathbf{g}}, \tag{7}$$

using U and L as characteristic velocity and length, respectively, g_0 as a characteristic source term, and the total viscosity $\eta_0 = \eta_s + \eta_p$.

Removing, for convenience, the bars in (7), the non-dimensional governing equations for isothermal incompressible flows of viscoelastic fluids are given by

$$\frac{\partial\mathbf{u}}{\partial t} + \nabla\cdot(\mathbf{uu}) = -\nabla p + \frac{\beta}{Re}\nabla^2\mathbf{u} + \frac{1}{Re}\nabla\cdot\mathbf{T} + \frac{1}{Fr^2}\mathbf{g}, \tag{8}$$

$$\nabla\cdot\mathbf{u} = 0, \tag{9}$$

$$\mathbf{T} + Wi\left(\frac{\partial\mathbf{T}}{\partial t} + (\mathbf{u}\cdot\nabla)\mathbf{T} - (\nabla\mathbf{u})\mathbf{T} - \mathbf{T}(\nabla\mathbf{u})^T\right) = 2(1-\beta)\mathbf{D}, \tag{10}$$

with non-dimensional groups: Reynolds number (Re), Weissenberg number (Wi), Froude number (Fr) and viscosity ratio ($\beta \in (0, 1]$) defined as

$$Re = \frac{\rho UL}{\eta_0}, \qquad Wi = \frac{\lambda_p U}{L}, \qquad Fr = \frac{U}{\sqrt{g_0 L}}, \qquad \beta = \frac{\eta_s}{\eta_0}. \tag{11}$$

2.1 Boundary conditions

In this work, we adopt a single-phase free surface formulation to model the interface dynamics, such that equations are solved only inside the liquid phase and boundary conditions are applied at the moving surface. These conditions are modeled by the normal and tangential stress equations, given, respectively, by

$$\mathbf{n}\cdot(\boldsymbol{\sigma}\cdot\mathbf{n}) = \gamma\kappa, \tag{12}$$

$$\mathbf{m}\cdot(\boldsymbol{\sigma}\cdot\mathbf{n}) = 0, \tag{13}$$

where $\mathbf{n}$ is the normal vector to the free surface, $\mathbf{m}$ is the tangential vector, γ is the surface tension coefficient, κ is the surface curvature, while the total stress tensor $\boldsymbol{\sigma}$ is

$$\boldsymbol{\sigma} = \boldsymbol{\tau} - p\mathbf{I} = 2\eta_s\mathbf{D} + \boldsymbol{\tau}^p - p\mathbf{I}. \tag{14}$$

We non-dimensionalize equations (12)-(13) using the same characteristic values as in (7), along with

$$\kappa = \frac{1}{L}\bar{\kappa}. \tag{15}$$

This way, equations (12)-(13) become

$$\mathbf{n} \cdot (\bar{\boldsymbol{\sigma}} \cdot \mathbf{n}) = \frac{1}{We}\bar{\kappa}, \tag{16}$$

$$\mathbf{m} \cdot (\bar{\boldsymbol{\sigma}} \cdot \mathbf{n}) = 0, \tag{17}$$

where

$$\bar{\boldsymbol{\sigma}} = 2\beta\bar{\mathbf{D}} + \bar{\mathbf{T}} - Re \cdot \bar{p}\mathbf{I}, \tag{18}$$

and We is the Weber number, given by

$$We = \frac{\rho U^2 L}{\gamma}. \tag{19}$$

From now on, the upper bars used for the non-dimensional variables will be dropped.

3 Overview of the numerical method

3.1 Projection method

In this work, the Navier-Stokes equations are solved numerically using the well-known projection method. In summary, this method uses the Helmhotz-Hodge decomposition to decouple velocity and pressure from equations (8)-(9).

The Helmhotz-Hodge decomposition [4] states that any vector field defined in a region Ω with smooth boundary $\partial\Omega$ can be uniquely decomposed as

$$\tilde{\mathbf{u}} = \mathbf{u} + \nabla\psi, \tag{20}$$

where $\mathbf{u}$ is a vector field such that $\nabla \cdot \mathbf{u} = 0$ and ψ a scalar field also defined in Ω.

The first step in the projection method is to solve the momentum equation (8) for an intermediate velocity field $\tilde{\mathbf{u}}$. In order to decouple velocity and pressure, we approximate the unknown p by some known scalar field $\tilde{p}$. The equation then becomes

$$\frac{\partial\tilde{\mathbf{u}}}{\partial t} + \nabla \cdot (\tilde{\mathbf{u}}\tilde{\mathbf{u}}) = -\nabla\tilde{p} + \frac{\beta}{Re}\nabla^2\tilde{\mathbf{u}} + \frac{1}{Re}\nabla \cdot \mathbf{T} + \frac{1}{Fr^2}\mathbf{g}, \tag{21}$$

where, for non-Newtonian flows, the tensor $\mathbf{T}$ is also assumed to be known.

Solving (21), we obtain a velocity field $\tilde{\mathbf{u}}$ for which, in general, the continuity equation is not yet satisfied. Using the Helmhotz-Hodge decomposition (20) and the continuity equation (9) we can create a Poisson equation for a scalar field ψ:

$$\nabla^2\psi = \nabla \cdot \tilde{\mathbf{u}}. \tag{22}$$

After solving equations (21) and (22) we have both $\tilde{\mathbf{u}}$ and ψ, such that the decomposition (20) can be used to obtain the final velocity field $\mathbf{u}$ that also satisfies the continuity equation. More details on this numerical treatment of the boundary conditions (16)-(17) can be seen in [1].

3.2 Discretization

The entire spatial domain is discretized using a uniform mesh, and the unknowns are evaluated on a staggered grid (velocity components on cell faces, pressure and stress on cell centers).

On top of the fixed grid, there will be a moving Lagrangian mesh which tracks the fluid interface. This mesh follows the classical Front-Tracking representation, which represents an interface using a number of connected marker particles. These markers are moved every timestep according to the velocity calculated on the underlying grid.

The cells on the fixed grid are classified according to their position with respect to the fluid interface. Each cell is classified as one of three possible options:

- EMPTY: a cell receives the EMPTY label if it does not contain any marker particles inside it and is located outside the region with fluid;
- SURFACE: a cell that contains at least one marker particle and that borders an EMPTY cell;
- FULL: these cells do not have EMPTY cells around its four faces, that is, they are inside a region with fluid.

Figure 1 shows a grid example with all its cells classified according to the fluid location. The Front-Tracking representation of the interface can also be seen through the connected marker particles.

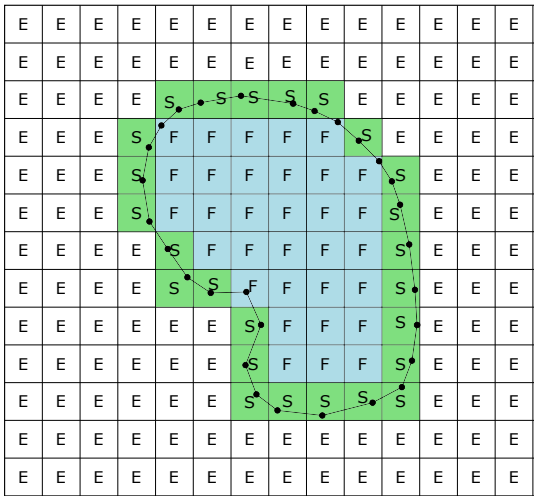

Figure 1. Example of cell classification in a free surface simulation.

The cell classification described above will determine which equations are solved in each of the grid points. For points inside FULL cells, for example, the momentum and Poisson equations are solved normally. For points inside EMPTY regions, nothing will be done, since there is no flow happening here. For points around SURFACE cells, the free surface boundary conditions will be used.

In order to use the boundary conditions in eqs. (16)-(17), we also need a value for the local interface curvature. The curvature is approximated by using the interface marker particles to fit a local parabola. The curvature of this parabola can be calculated exactly and is used as an approximation for the interface.

4 Numerical results: binary droplet collision

Binary droplet collisions are of interest in many different applications such as raindrop formation, nuclear fusion and various spraying processes according to Qian and Law [5]. Due to its complexity, this problem has been studied in the literature for decades, but questions still remain open. Ashgrin and Poo [6], for example, carry out experiments with water drops colliding in an air medium and the authors are able to capture three different types of coalescence regimes. In [5] new experiments are performed using tetradecane droplets inside a nitrogen (gas) medium. These authors were able to show that, unlike water, tetradecane droplets do not always coalesce after impact, instead they can bounce away from each other. In general, three impact regimes are usually considered for binary drop collisions:

- bouncing: the droplets collide and bounce away from each other without merging;
- total coalescence: the two droplets collide and permanently merge into one;
- separation: the droplets initially coalesce into one, which stretches heavily eventually breaking up again.

When it comes to numerical simulations, the problem of binary droplet collision is considered extremely complex, mainly due to its topological changes. Methods that represent the interface purely implicitly, e.g. Volume-of-Fluid, automatically join the two droplets when they get close to each other, resulting in coalescence [7]. This implicit approach is used in the works of Li et al. and Nikolopoulos et al. [8, 9] among many others. On the other hand, methods that describe the interface explicitly, e.g. Front-Tracking, never automatically join the two droplets, which causes them to always bounce from each other. This approach has been used in [10, 11].

In this problem, both droplets are initialized with given velocities $\mathbf{u}_1$ and $\mathbf{u}_2$, respectively, and the initial geometry can be defined by a single impact parameter B, given by

$$B = \frac{b}{D}, \tag{23}$$

where D is the diameter of the droplets and b is the center-to-center relative distance as illustrated in Figure 2. Note that $B = 0$ represents head-on impact, while $B = 1$ indicates a grazing collision. The nondimensionalization is performed using the diameter (D) and relative velocity ($|\mathbf{u}_r|$) as characteristic length and velocity, respectively.

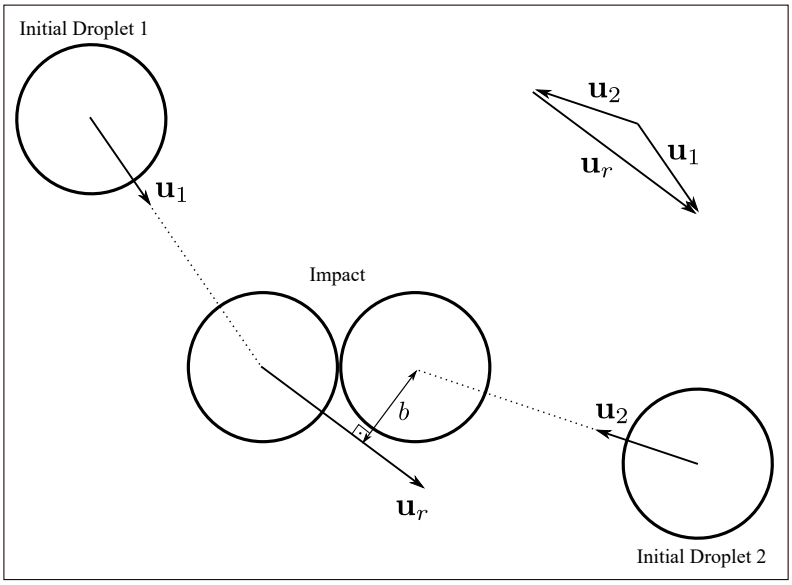

Figure 2. Schematic of the geometry used in the binary droplet collision simulations.

In our study we are interested in investigating how elasticity can affect the behaviour in the droplet collisions. Below we will show results for each of the three possible outcomes: bouncing, coalescence and separation. The parameters used for each case are presented in table 1.

Table 1. Data used in the simulations

Case	Velocity (m/s)	Diameter (m)	ρ (kg/m^3)	η_0 (Pa $\cdot$ s)	γ (N/m)	Reynolds	Weber
Bouncing	1.106	0.000375	998	0.0082	0.0458	50.48	10
Coalescence	1.916	0.000375	998	0.0082	0.0458	87.45	30
Separaton	2.473	0.000375	998	0.0082	0.0458	112.89	50

We begin by showing a simulation that falls into the bouncing regime. Figure 3 shows the side-by-side comparison between a Newtonian and a viscoelastic simulation for the bouncing case. We notice that the viscoelastic droplets suffer a bigger deformation during impact. To illustrate this more clearly, Figure 4 shows the maximum radius of one of the droplets over time. The viscoelastic droplet clearly deforms more at the momemnt of impact and continues to oscillate for much longer than the Newtonian one, which quickly stabilizes into a circular shape.

We continue by investigating a case resulting in the coalescence regime. Figure 5 shows a comparison of time frames between a Newtonian and a viscoelastic simulation in this case. Once again, we note that the viscoelastic droplet deforms and stretches more than its Newtonian counterpart.

Finally, in Fig. 6 we also show a Newtonian-viscoelastic comparison for a simulation resulting in separation. In this particular case, the effect of elasticity is so relevant that it even changes the final outcome of the simulation, that is, while the Newtonian droplet separates, the viscoelastic one coalesces permanently.

5 Conclusions

The behaviour presented by small droplets during collision was studied in this work. In particular, we have focused on showing the differences caused by the presence of elasticity in the droplet fluid. While the results introduced here are still preliminary, we were already able to see that elasticity can have a very significant effect on the flow dynamics, greatly modifying the droplet deformation.

We intend to continue this study by further investigating how elasticity can change the final collision outcome (bouncing, coalescence, stretching), with the intent of creating a numerical method that can correctly predict the correct outcome based on the viscoelastic fluid and flow parameters.

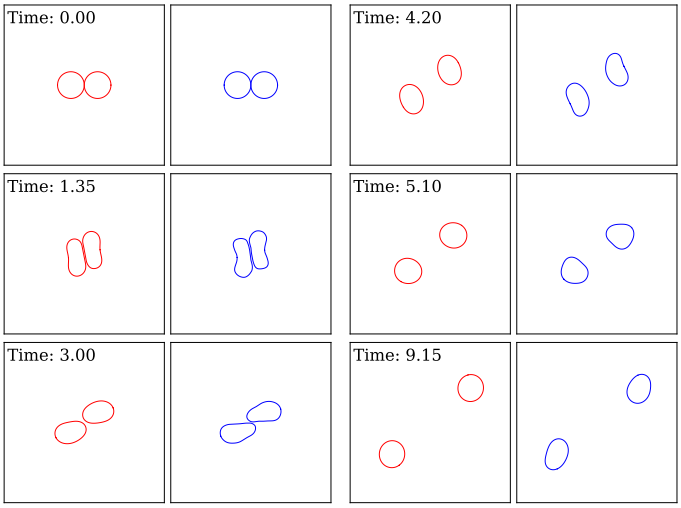

Figure 3. Bouncing case. Parameters: $Re = 50.48$, $We = 10$ and $B = 0.2$. Red: Newtonian and Blue: Oldroyd-B with $Wi = 5$, $\beta = 1/9$.

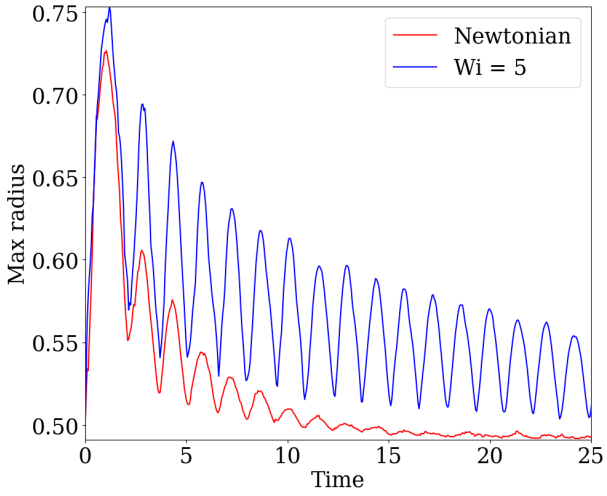

Figure 4. Max radius over time for a bouncing simulation.

Acknowledgements. The authors would like to thank the financial support given by FAPESP grants no. 2013/07375-0 and 2019/01811-9.

Authorship statement. The authors hereby confirm that they are the sole liable persons responsible for the authorship of this work, and that all material that has been herein included as part of the present paper is either the property (and authorship) of the authors, or has the permission of the owners to be included here.

References

[1] C. M. Oishi, R. L. Thompson, and F. P. Martins. Transient motions of elasto-viscoplastic thixotropic materials subjected to an imposed stress field and to stress-based free-surface boundary conditions. *International Journal of Engineering Science*, vol. 109, pp. 165 – 201, 2016.

[2] C. M. Oishi, R. L. Thompson, and F. P. Martins. Normal and oblique drop impact of yield stress fluids with thixotropic effects. *Journal of Fluid Mechanics*, vol. 876, pp. 642–679, 2019.

[3] D. Izbassarov, M. E. Rosti, M. N. Ardekani, M. Sarabian, S. Hormozi, L. Brandt, and O. Tammisola. Computational modeling of multiphase viscoelastic and elastoviscoplastic flows. *International Journal for Numerical Methods in Fluids*, vol. 88, n. 12, pp. 521–543, 2018.

[4] A. Chorin and J. Marsden. *A mathematical introduction to fluid mechanics*. Springer-Verlag, 1979.

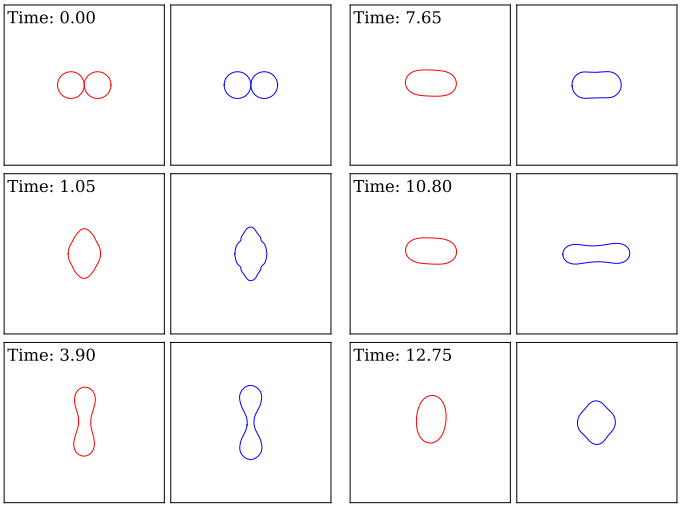

Figure 5. Coalescence case. Parameters: $Re = 87.45$, $We = 30$ and $B = 0$. Red: Newtonian and Blue: Oldroyd-B with $Wi = 5$, $\beta = 1/9$.

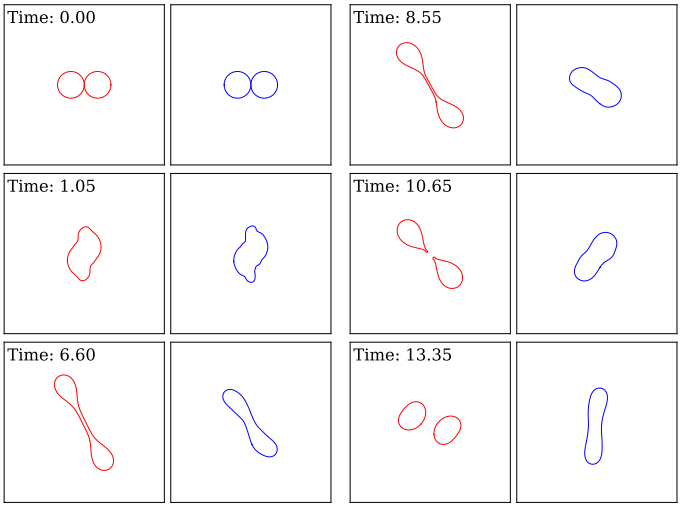

Figure 6. Separation case. Parameters: $Re = 112.89$, $We = 50$ and $B = 0.5$. Red: Newtonian and Blue: Oldroyd-B with $Wi = 3$, $\beta = 1/9$.

[5] J. QIAN and C. K. LAW. Regimes of coalescence and separation in droplet collision. *Journal of Fluid Mechanics*, vol. 331, pp. 59–80, 1997.
[6] N. Ashgriz and J. Y. Poo. Coalescence and separation in binary collisions of liquid drops. *Journal of Fluid Mechanics*, vol. 221, pp. 183–204, 1990.
[7] G. Finotello, J. T. Padding, N. G. Deen, A. Jongsma, F. Innings, and J. A. M. Kuipers. Effect of viscosity on droplet-droplet collisional interaction. *Physics of Fluids*, vol. 29, n. 6, pp. 067102, 2017.
[8] X. G. Li and U. Fritsching. Numerical investigation of binary droplet collisions in all relevant collision regimes. *The Journal of Computational Multiphase Flows*, vol. 4, n. 4, pp. 207–224, 2011.
[9] N. Nikolopoulos, A. Theodorakakos, and G. Bergeles. Off-centre binary collision of droplets: A numerical investigation. *International Journal of Heat and Mass Transfer*, vol. 52, n. 19-20, pp. 4160–4174, 2009.
[10] M. R. H. Nobari and G. Tryggvason. Numerical simulations of three-dimensional drop collisions. *AIAA Journal*, vol. 34, n. 4, pp. 750–755, 1996.
[11] M. R. Nobari, Y.-J. Jan, and G. Tryggvason. Head-on collision of drops—a numerical investigation. *Physics of Fluids*, vol. 8, n. 1, pp. 29–42, 1996.